International Journal of Biological Macromolecules 111 (2018) 706–716

Contents lists available at ScienceDirect

International Journal of Biological Macromolecules

journal homepage: https://www.journals.elsevier.com/biomac

Green synthesis of antimicrobial and antitumor *N*,*N*,*N*-trimethyl chitosan chloride/poly (acrylic acid)/silver nanocomposites

Mahmoud H. Abu Elella [a], Riham R. Mohamed [a,*], Marwa M. Abdel-Aziz [b], Magdy W. Sabaa [a]

[a] Chemistry Department, Faculty of Science, Cairo University, Giza 12613, Egypt
[b] The Regional Center for Mycology and Biotechnology, Azhar University, Cairo 11651, Egypt

ARTICLE INFO

Article history:
Received 20 October 2017
Received in revised form 27 November 2017
Accepted 9 January 2018
Available online 13 January 2018

Keywords:
N,*N*,*N*-trimethyl chitosan chloride
Poly(acrylic acid)
Polyelectrolyte complex
Nanocomposites
Antimicrobial activity

ABSTRACT

The present study is imported to solve two critical problems we face in our daily life which are microbial pollution and colon cancer. One pot green synthesis of a water soluble polyelectrolyte complex (PEC) between cationic polysaccharide as *N*,*N*,*N*-trimethyl chitosan chloride (TMC) and anionic polymer as poly (acrylic acid) (PAA) in presence of silver nanoparticles to yield (TMC/PAA/Ag) nanocomposites with different Ag weight ratios. Structure of TMC, PAA and TMC/PAA (PEC) were proved via different analysis tools. TMC/PAA and its Ag nanocomposites are used as antimicrobial agents against different pathogenic bacteria and fungi to solve microbial pollution. TMC/PAA-Silver nanocomposites had the highest antimicrobial activity which increases with increasing Ag %. Cytotoxicity data confirmed also that TMC/PAA/Ag (3%) had the most cytotoxic effect (the less cell viability %) towards colon cancer. TMC/PAA (PEC) was formed through electrostatic interactions between *N*-quaternized (-N^+R_3) groups in TMC and carboxylate (-COO^-) groups in PAA.

1. Introduction

Microbial pollution is considered as one of the major problems that concerns health worldwide. It is caused by pathogenic microbes via different diseases including diarrhea, abdominal pain, nausea, vomiting, hemorrhagic colitis and hemolytic uremic syndrome, pyogenic liver abscess, meningitis and pneumonia. Pathogenic bacteria such as *Staphylococcus aureus* (*S. aureus*) and *Bacillis subtilis* (*B. subtilis*) are *Gram positive bacteria*, while, *Escherichia coli* (*E. coli*) and *Klebsiella pneumoniae* (*K. pneumoniae*) are *Gram negative bacteria*. Moreover, pathogenic fungi may include *Geotricum candidum* (*G. candidum*) and *Aspergillus fumigatus* (*A. fumigates*). Researchers exert great efforts to develop effective antimicrobial agents to control microbial pollution [1–5]. In past decades, metal nanoparticles were of interest to material science researchers, as they were used in different fields as; catalysis [6, 7], biosensing [8], antimicrobial [9, 10], cancer therapies [11],…etc.

Cancer is a global problem threatening human life as it involves abnormal cell division [12]. Colorectal cancer (CRC) is known as human colon cancer and it is considered the third most dangerous cancer type [13]. It spreads in many countries such as United States, Korea, China and Japan [14, 15]. However, in Egypt, previous studies showed that colon cancer patients under age 30, 40 and 50 represent 20%, 35% and 59%, respectively, of the total colon cancer patients in Egypt [15]. In 2015, it was diagnosed in over one million people and caused death to 608,700 persons worldwide [16, 17].

Silver nanoparticles, AgNPs, are considered one of the important noble metal nanoparticles that are used in biological fields as antimicrobial agents, due to their inhibitory effect against pathogenic microorganisms [10, 18–20]. Also, they are added to skin ointments and creams to heal burns and wounds infection [19]. Recently, AgNPs were used in cancer therapy [21]. AgNPs were synthesized via reduction using reducing agents [22]. However, the reducing agents are highly reactive and having both biological and potential environmental risks [23].

Green synthesis of AgNPs has been reported using non-toxic reducing agents such as living organisms, plant leaves and seed extracts [24–26]. Recently, they were synthesized by natural polysaccharides including chitosan, agar, locust bean gum and xanthan gum as mild reducing agents depending on hydroxyl groups (-OH) on its backbone. Polysaccharides are low cost, nontoxic and biocompatible reducing agents [23, 27].

This study aims to synthesize water soluble polyelectrolyte complex (PEC) via electrostatic interactions between *N*,*N*,*N*-trimethyl chitosan chloride (TMC) and poly (acrylic acid) (PAA) in acidic conditions to "green" synthesize AgNPs forming water soluble nanocomposites (TMC/PAA/Ag) with potential antimicrobial and antitumor activities. TMC was synthesized by reacting chitosan (Ch), which is a cationic polysaccharide, with a methylating agent like dimethyl sulfate $(CH_3)_2SO_4$ [28, 29].

* Corresponding author.
E-mail address: rihamrashad@sci.cu.edu.eg (R.R. Mohamed).

https://doi.org/10.1016/j.ijbiomac.2018.01.055
0141-8130/

TMC has excellent properties including; non-toxicity, biodegradability, biocompatibility, antimicrobial activity [9, 30]. While, PAA is an anionic water soluble synthetic polymer, having carboxyl (-COOH) groups along its backbone [31]. PAA has a good antibacterial activity and used as a stabilizing agent during preparation of AgNPs [31–33].

TMC/PAA (PEC) and TMC/PAA/Ag nanocomposites were synthesized in different weight ratios of Ag (1%, 2% and 3%) then were characterized via different analysis tools and were examined as antimicrobial agents against pathogenic microorganisms as well as antitumor agents against Human Colon cancer cell.

2. Materials & methods

2.1. Materials

Chitosan (Ch) was purchased from Oxford-London, UK (DD 90–95%) and the viscosity average molecular weight was 160,000 g mol^{-1}. Poly (acrylic acid) (PAA) (25 wt% aqueous solution) was purchased from Alfa Aesar®-Germany (Average molecular weight = 210,000 g mol^{-1}). Sodium chloride (NaCl), sodium hydroxide (NaOH), hydrogen chloride (HCl) and silver nitrate ($AgNO_3$) were purchased from Merck-Germany. Dimethyl sulfate ($(CH_3)_2SO_4$) was purchased from Lobachemi Pvt. Ltd., Mumbai-India. Visking® dialysis tubing regenerated cellophane (Molecular weight cut off 12,000–14,000 g mol^{-1}) was purchased from Serva Electrophoresis, Heidelberg-Germany. *Staphylococcus aureus* (*S. aureus*, RCMB 010028) and *Bacillus subtilis* (*B. subtilis*, RCMB 010067) as *Gram-positive* bacteria, *Escherichia coli* (*E. coli*, RCMB 010052) and *Klebsiella pneumoniae* (*K. pneumoniae*, RCMB 010093) as *Gram- negative* bacteria and Aspergillus fumigatus (*A. fumigatus*, RCMB 02568), *Geotricum candidum* (*G. candidum*, RCMB 05097) as fungi, were provided by the regional center for mycology and biotechnology Azhar University-Egypt. Human colon cancer cell lines (HCT-116) and Mammalian cell lines (African green monkey kidney cell lines (VERO cells)) were obtained from VACSERA-Tissue Culture Unit. Crystal violet and trypan blue dye were purchased from Sigma Aldrich, Germany. Fetal bovine serum, L-glutamine, gentamycin, Dulbecco's modified Eagle's medium (DMEM) and 4-(2-hydroxyethyl)-1-piperazine ethane sulfonic acid (HEPES) buffer solution were purchased from Lonza, Basel - Switzerland.

2.2. Methods

2.2.1. Preparation of N,N,N-trimethyl chitosan chloride (TMC)

N,N,N-trimethyl chitosan chloride (TMC) was prepared via de Britto D. et al. method [34]. Briefly, 2 g of Ch was suspended in 32 mL of dimethyl sulfate and 8 mL of dist. Water then was stirred for 15 min then both NaOH solution (2.4 g/10 mL distilled water) and 1.78 g NaCl were added dropwisely to Ch solution during 10 min. After that, the solution was stirred well for 6 h at room temperature (~25 °C). Purify the resulting product using dialysis tubing regenerated cellophane (molecular weight cut off 12,000–14,000 g mol^{-1}) in distilled water for three days. The final product was obtained by precipitation in acetone then filtration. Finally, the product was dried under vacuum (Scheme 1). The structure of TMC was elucidated using ^{1}H-NMR and FTIR analysis.

2.2.2. Preparation of water soluble TMC/PAA polyelectrolyte complex

1.0 g of TMC was dissolved in 100 mL of distilled water and the pH of this solution was adjusted to 2.0 using 0.1 M HCl then it was added dropwisely to a solution of PAA (1.0 g/100 mL of distilled water) and stirred for 1 h at 30 °C. The final product was precipitated in acetone then it was filtered and dried in vacuum oven at 40 °C for 24 h till constant weight (Scheme 1). TMC/PAA was designated as polyelectrolyte complex (PEC) [35].

2.2.3. Preparation of TMC/PAA/Ag nanocomposites

PEC (TMC/PAA) (1 g) was dissolved in 10 mL of distilled water in a round-bottomed flask (25 mL) under constant stirring. Different quantities of $AgNO_3$ were dissolved in less amount of distilled water then it was added slowly to the previous solution in dark conditions with continuous stirring at room temperature for 24 h to yield different percentages of Ag nanoparticles (1%, 2% and 3%)-Scheme (1). The color of PEC turned from light yellow into dark brownish yellow after adding $AgNO_3$ which indicated the reduction of Ag ions to Ag NPs inside the polymer matrix [9, 23, 36].

2.2.4. In vitro antimicrobial activity

Agar well diffusion method [37] was used for in vitro antimicrobial activity measurements for TMC, PAA, TMC/PAA (PEC) and TMC/PAA/Ag nanocomposites against *Staphylococcus aureus* (RCMB 010028) and *Bacillus subtilis* (RCMB 010067) as *Gram-positive* bacteria and against *Escherichia coli* (RCMB 010052) and *Klebsiella pneumoniae* (RCMB 010093) as *Gram-negative* bacteria using nutrient agar medium and against *Aspergillus fumigatus* (RCMB 02568) and *Geotricum candidum* (RCMB 05097) as pathogenic fungi using sabouraud dextrose agar medium in presence of Ampicillin as reference drug for *Gram-positive* bacteria, Gentamicin as reference drug for *Gram-negative* bacteria and Amphotericin B as reference drug for fungi. The well diameter was 6 mm (mm) using 1 mg mL^{-1} from tested samples and reference drugs in presence of water as solvent control. For bacteria, the plates were incubated at 37 °C for 24 h, while, the incubation was 48 h at 25 °C for fungi. After incubation, the diameter of the inhibition zones of microbial growth for tested samples was measured and was compared with that of the reference drugs. Its values were the average of three reproducible experiments and expressed as mean (± standard deviation) (SD). The minimum inhibitory concentration (MIC), which is the lowest concentration of an antimicrobial agent that will inhibit the visible growth of a microorganism after overnight incubation, was determined by the brain heart infusion broth micro dilution method using 96-well micro-plates [38, 39].

The inoculated of the microbial strains was prepared from 24 h broth cultures and suspensions were adjusted to 0.5 McFarland standard turbidity (10^5 CFU mL^{-1}). 1.0 mg of tested samples was dissolved in 1.0 mL H_2O to obtain 1000 μg mL^{-1} stock solution, positive and negative controls were included in each plate. Sterile broth (100 μL) was added to the well from row B to H, while, the stock solutions of samples (100 μL) were added to the wells in rows A and B. The mixture of samples and sterile broth (100 μL) in row B were transferred to each well in order to obtain a twofold serial dilution of the stock samples (500, 250, 125, 62.5, 31.30, 15.60, 7.81, 3.90, 1.95, 0.98 and 0.49 μg mL^{-1}). For antibacterial activity, plates were incubated at 37 °C for 24 h. However, for antifungal activity, they were incubated at 25 °C for 48 h. Microbial growth was evaluated by the presence of turbidity and the pellet was at the bottom of the well. ELISA reader device was used for measuring the optical density of each well at 520 nm.

2.2.5. Antitumor activity

Human colon cancer (HCT-116) cell lines were propagated in Dulbecco's Modified Eagle's Medium (DMEM) supplemented with 10% fetal bovine serum, 1% L-glutamine, 4-(2-hydroxyethyl)-1-piperazine ethane sulfonic acid (HEPES) buffer and 50 μg mL^{-1} Gentamycin, then they were maintained in a humidified atmosphere with 5% CO_2 at 37 °C. They were subcultured two to three times a week. For cell viability assays, HCT-116 cell lines were seeded in medium at a cell concentration of 1×10^4 cells/well in 96-well plates then fresh medium contains various concentrations of tested polymer samples (TMC/PAA (PEC), TMC/PAA/1% Ag and TMC/PAA/3% Ag) using H_2O as solvent was added to previous seeded cells after 24 h. Two-fold serial dilutions (3.9, 7.8, 15.6, 31.25, 62.5, 125, 250, 500, 1000 μg mL^{-1}) of the tested samples were added to confluent cell monolayers dispensed into 96-well, flat-bottomed microliter plates using a multichannel pipette which were incubated at 37 °C in a humidified incubator with 5% CO_2

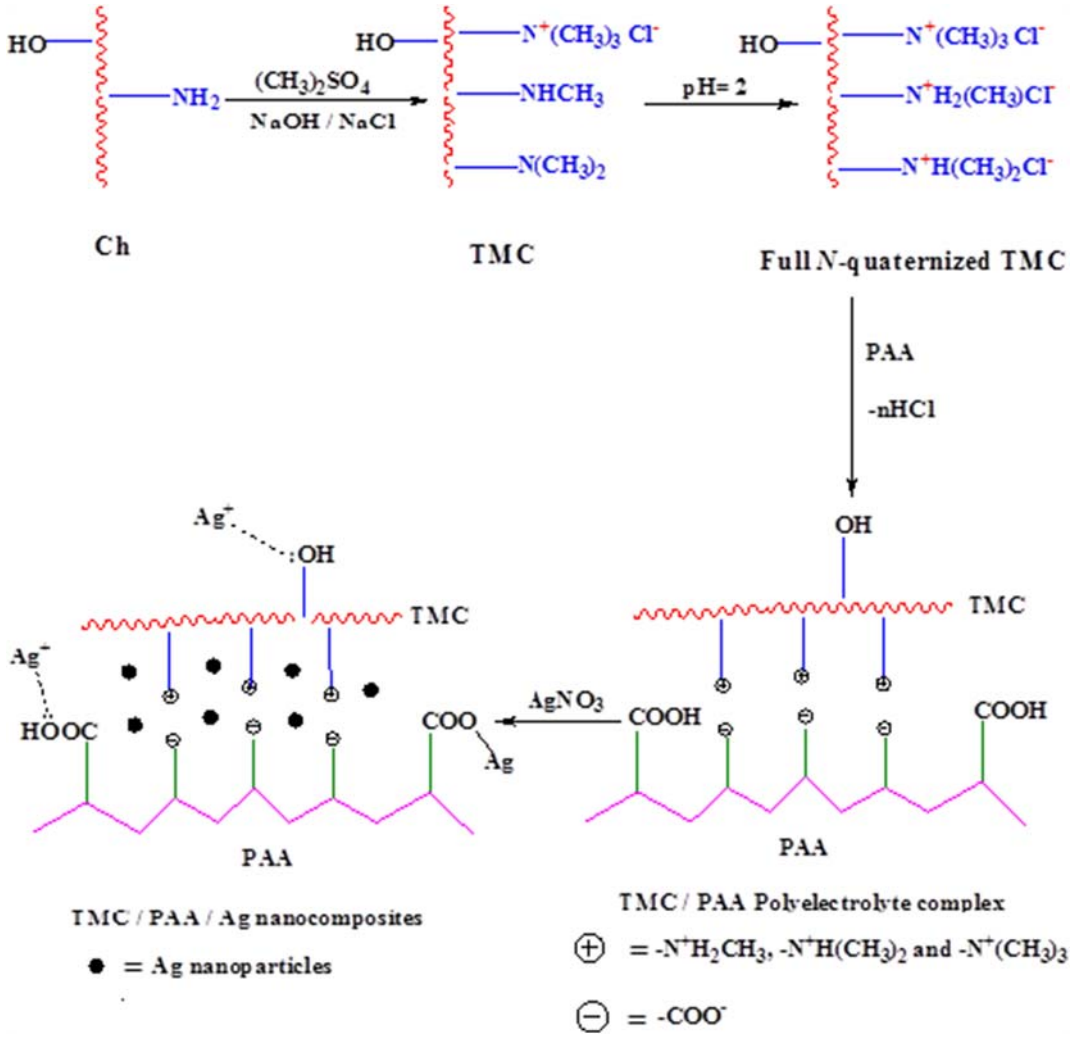

Scheme 1. Preparation of TMC, TMC/PAA (PEC) and TMC/PAA/Ag nanocomposites.

for a period of 48 h. After incubation, different concentrations of tested samples were added, and the incubation was continued for 24 h at 37 °C and yield of cell viability was determined by a colorimetric method. After incubation, 1% crystal violet solution was added to each well for at least 30 min. All experiments were carried out in triplicates and cell viability of each tested sample was calculated according to its optical density. The optical density was measured with the microplate reader at 490 nm to determine the percentage of cell viability according to the following equation:

$$\text{Cell Viability}\% = [1-(\text{ODt}/\text{ODc})] \times 100$$

Where, ODt is the mean optical density of wells treated with the tested sample and ODc is the mean optical density of untreated cells. The cytotoxicity effect of TMC/PAA/Ag(3%) nanocomposite on African green monkey kidney cell lines (VERO cells) was performed by the same method. The half maximum inhibitory concentrations (IC_{50}) of tested samples, which is defined as the sample concentration required to cause toxic effects in 50% of intact cells, were estimated in every case from dose response curve, it is the relation of cell viability % of tested samples and its concentration, using Graphpad Prism software (San Diego, CA. USA) [40, 41].

3. Instrumentation

Proton Nuclear Magnetic Resonance (^{1}H-NMR) spectra of tested samples (Ch, TMC, PAA and TMC/PAA PEC) were scanned by Varian Mercury VX-300 NMR Spectrometer and its spectra were run at 300 MHz in DMSO/Trifluoroacetic acid (TFA) as solvent for Ch and D_2O as solvent for remaining samples. Fourier Transform Infrared (FTIR) spectra of tested samples were recorded using Jasco FTIR 4100 spectrometer (Japan) through the frequency range of 600–4000 cm^{-1}. Diameter of prepared AgNPs was examined by High Resolution Transmission Electron Microscope (HR-TEM), Tecnai G20, FEI, Netherland. The surface morphology of TMC, TMC/PAA (PEC) and nanocomposites samples was examined by a field emission scanning electron microscope, FE-SEM (Quanta 250 FEG). The elemental analysis of TMC/PAA/3% Ag was studied with energy dispersive X-Ray analyses (EDX) unit that is attached with FE-SEM and set up with energy 5.4 kev. X–Ray Diffraction (XRD) spectra of TMC, TMC/PAA (PEC) and TMC/PAA/Ag nanocomposite were obtained using an X–ray powder diffractometer (X'Pert PRO with secondary monochromator, Cu-radiation ($\lambda = 1.542$ Å) at 45 K.V., 35 M.A. and scanning speed $0.02°\cdot s^{-1}$). The diffraction peaks between $2\theta = 4° - 70°$.

4. Results & discussion

4.1. Proton nuclear magnetic resonance (^{1}H-NMR) spectroscopy

Synthesis of TMC and water-soluble TMC/PAA PEC was proven using ^{1}H-NMR spectra-Fig. 1(a,b) which showed the main signals of Ch and TMC. ^{1}H-NMR spectrum of Ch was discussed previously by the same authors [32] as it showed two singlet signals at $\delta = 1.8$ and 2.8 ppm

corresponded to protons of the methyl (–CH_3) group of the remained *N*-acetyl (-$NHCOCH_3$) groups and protons bonded to C_2 of *N*-glucosamine and *N*-acetyl glucosamine, respectively [42, 43]. In addition, multiplet signal at $\delta = 3.5–3.8$ ppm assigned to protons bonded to C_3, C_4, C_5 and C_6 of glycopyranose unit [H_3,H_4,H_5 and H_6] and two singlet signals at $\delta = 4.7$ and 8.3 ppm referred to protons bonded to anomeric C_1 of glycopyranose unit [H_1] and protons of amino (-NH_2) groups, respectively [34, 42, 44, 45]. Moreover, two sharp signals appeared at $\delta =$ 2.5 and 9.6 ppm related to dimethyl sulphoxide (DMSO) and trifluoroacetic acid (TFA), respectively, as solvents. While, ^{1}H-NMR spectrum of TMC showed singlet signal at $\delta = 1.9$ ppm referred to protons of remaining *N*-acetyl glucosamine units, also, it showed a low intensity singlet signal at $\delta = 2.8$ ppm corresponded to protons of monomethyl amino (-$NH(CH_3)$) groups and sharp singlet signals at 3.0 and 3.2 ppm related to both protons of dimethyl amino (-$N(CH_3)_2$) groups and protons of *N*-quaternized amino (-$N^+(CH_3)_3$) groups, respectively. Moreover, low intensity singlet signal at $\delta = 3.3$ assigned for protons of methyl group which are connected to oxygen No. 6 (O^6-CH_3), this is an evidence on the synthesis of TMC with low degree of O-methylation using $(CH_3)_2SO_4$. In addition to that, multiplet signals appeared at $\delta = 3.6–4.2$ ppm were attributed to protons bonded to C_3, C_4, C_5 and C_6 of glycopyranose unit [H_3,H_4,H_5 and H_6] and multiplet signals appeared at $\delta = 5.0–5.3$ ppm corresponded to proton bonded to anomeric C_1 of glycopyranose unit [H_1]. Furthermore, singlet signal at $\delta = 8.3$ ppm referred to protons of amino (-NH_2) groups disappeared in TMC spectrum, as TMC did not have remaining amino groups [34, 45–47]. There were sharp signals at $\delta = 4.6$ ppm related to D_2O as a solvent.

N-Quaternization percentage (DQ%) in TMC was calculated from the following equation:

$$DQ\ (\%) = \left[\left(-N^+(CH_3)_3\right)/9\right]/[H_1] \times 100$$

Where; [(-N^+ $(CH_3)_3$)] corresponded to the integral area under the signal of the *N*,*N*,*N*-trimethyl protons at $\delta = 3.2$ ppm and [H_1] related to integral area under the signal of H_1 proton at $\delta = 5.0–5.3$ ppm [45]. DQ% of TMC was calculated as 70%.

Furthermore, ^{1}H-NMR spectrum of PAA (Fig. 1c) showed main characteristic signals of PAA. Triplet signal at $\delta = 1.7–2.0$ ppm referred to protons of methylene (-CH_2) groups and singlet signal at $\delta = 2.5$ ppm corresponded to proton of methine (-CH) groups on the backbone of PAA. In addition to, a sharp singlet signal at $\delta = 4.8$ ppm related to D_2O as a solvent [48]. Moreover, Fig. 1(d) showed ^{1}H-NMR spectrum of TMC/PAA (PEC). This spectrum exhibited characteristic signals of

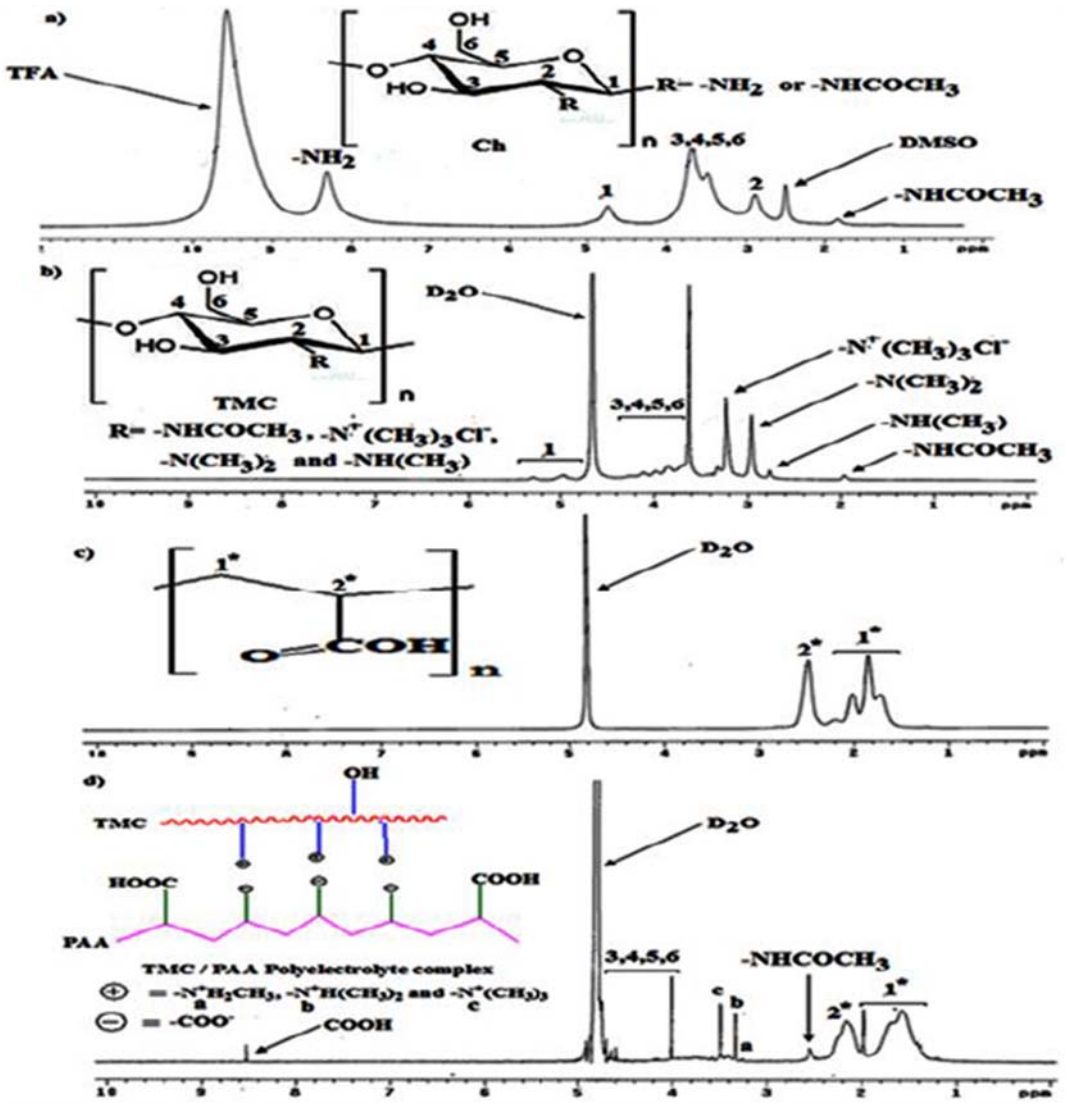

Fig. 1. ^{1}H-NMR of a) Chitosan b) TMC c) PAA d) TMC/PAA.

both TMC and PAA. Signals at δ = 1.5–2.2 ppm related to protons of both methylene (-CH_2) and methine (-CH) groups in PAA. These signals were shifted to less chemical shifts than their original values in Fig. 1(c), because of the consumption of carboxylic acid (-COOH) groups in the formation of (PEC) with TMC. While, signals of TMC appeared at δ = 2.5 ppm assigned to protons of remaining *N*-acetyl glucosamine units, at δ = 3.2 ppm assigned to protons of quaternization of monomethyl amino (-$N^+H_2(CH_3)$) groups, at δ = 3.3 ppm assigned to protons of quaternization of dimethyl amino (-$N^+H(CH_3)_2$) groups and at δ = 3.3 ppm assigned to protons of *N*-quaternized amino (-$N^+(CH_3)_3$) groups. Also, multiplet signal at δ = 4.0–4.7 ppm attributed to protons bonded to C_3, C_4, C_5 and C_6 of glycopyranose unit [H_3,H_4,H_5 and H_6] and signal at δ = 4.9–5.0 ppm corresponded to proton bonded to anomeric C_1 of glycopyranose unit [H_1]. However, sharp signal at δ = 4.8 ppm related to solvent (D_2O) and small signal at δ = 8.5 ppm assigned to remaining carboxylic acid groups on PAA backbone.

4.2. Fourier transform infrared (FTIR) spectroscopy

FTIR spectra (Fig. 2a) illustrated the main peaks of Ch and TMC. It had proven the synthesis of TMC and its comparison to Ch. The spectrum of Ch was reported by the same authors [32] and it showed the main peaks of Ch described as follows: absorption peak at 3435 cm^{-1} due to stretching vibration of O—H and N—H bonds and this peak was broad due to the H-bonding interactions. In addition to, absorption peaks at 2918 and 2879 cm^{-1} assigned to symmetric stretching vibrations of alkyl (C—H) groups, while absorption peaks at 1653 and 1597 cm^{-1} corresponded to stretching vibration of carbonyl (C═O) bond of the remaining *N*-acetyl groups (-$NHCOCH_3$) and N—H bending vibration of amino (-NH_2) groups, respectively [34, 49, 50]. Moreover, absorption peaks around 1155 and 895 cm^{-1} corresponded to C—O—C bending vibration in saccharide repeated unit in Ch and broad peaks at 1080 and 1031 cm^{-1} assigned for C—OH stretching vibration of 2nd and 1^{ry} alcohol on the backbone, respectively [34, 49, 51]. On the other hand, FTIR spectrum of TMC showed a broad peak at 3435 cm^{-1} related to stretching vibration of both O—H and N—H bonds, however, it has less intensity than the same peak in Ch as it is converted to different groups like; -NH (CH_3), -N (CH_3)$_2$ and -N^+ (CH_3)$_3$, so the hydrogen bonding interactions between O—H and N—H decreased between TMC chains. This in addition to the new peak appeared at 1647 cm^{-1} corresponded to the -C═O stretching vibration of remaining N-acetyl groups [51]. Furthermore, new absorption peak appeared at 1465 cm^{-1} assigned for the bending vibration of methyl groups of *N*-alkylated (-NH (CH_3), -N(CH_3)$_2$ and -N^+(CH_3)$_3$) groups in TMC [52].

FTIR spectra (Fig. 2b) showed the main peaks of PAA, TMC and TMC/PAA (PEC). FTIR spectrum of PAA showed a broad peak at 3432 cm^{-1} resulted from H-bonding interactions between hydroxyl (-OH) groups of carboxylic acid on PAA backbone [31] and absorption peak exhibited at 1710 cm^{-1} corresponded to carbonyl (-CO) stretching vibration in carboxylic acid groups [53]. Moreover, two absorption peaks appeared at 1632 and 1450 cm^{-1} related to symmetric and asymmetric stretching vibration of carboxylate (-COO^-) groups [54]. FTIR spectrum of TMC/PAA (PEC) showed a broad absorption peak at 3432 cm^{-1} corresponded to –OH and –NH groups in TMC and –OH groups in PAA. In addition to two peaks at 1710 and 1647 cm^{-1} related to carbonyl (-C═O) stretching vibration of carboxylic acid in PAA and remaining *N*-acetyl groups in TMC, respectively. Sharp absorption peak appeared at 1553 cm^{-1} attributed to carboxylate (-COO^-) stretching vibration groups, also sharp peak at 1416 cm^{-1} related to bending vibration of –CH bonds in methyl groups of *N*-quaternized (-$N^+H_2(CH_3)$, $N^+H(CH_3)_2$ and -$N^+(CH_3)_3$) groups in TMC that shifted from 1465 cm^{-1} in TMC to 1416 cm^{-1} through PEC formation with PAA via H-bonding interactions between *N*-quaternized groups in TMC and carboxylate groups in PAA. The FTIR spectrum of synthesized TMC/PAA/Ag nanocomposites (Fig. 2c) exhibited shift stretching vibrations peaks of TMC/PAA (PEC) due to coordination bond/electrostatic attraction between Ag^+ ions and hydroxyl and carboxylate ions present in PEC during formation of Ag nanoparticles, this observation was in agreement with literature [36, 55, 56].

4.3. Scanning electron microscopy (SEM)

Surface morphology of Ch, TMC, TMC/PAA (PEC) and TMC/PAA/Ag nanocomposites was examined via scanning electron microscopy (SEM) with magnification (×500) and their images were illustrated in Fig. (3). The surface of Ch appeared as large regular crystalline structure, as a result of the strong intermolecular H-bonding interactions between its chains [57]. While, the surface of TMC appeared smooth due to destruction of these intermolecular H-bonding and insertion of *N*-methyl groups into TMC chains led to destruction of the crystallinity of Ch, this observation was in agreement to literature [35]. Moreover, TMC/PAA (PEC) surface was rough and porous with globular shape due to the presence of carboxylic and *N*-quaternized groups on PEC chains and formation of electrostatic interactions between both of them, this was shown obviously in a small inserted image with magnification (×5000).

However, surface of TMC/PAA/Ag nanocomposites appeared rough porous with lustrous Ag particles imbedded within the matrix, Ag NPs were referred in a separated image with magnification

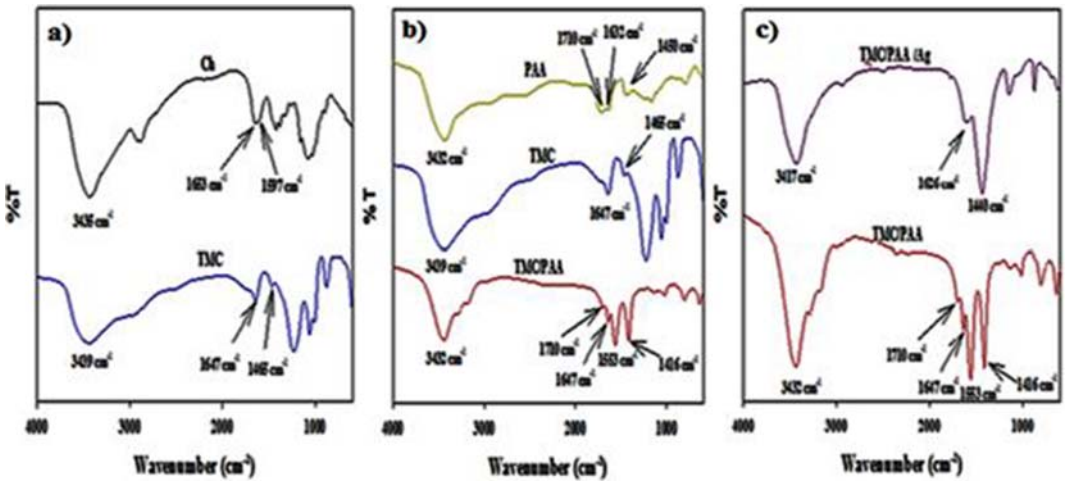

Fig. 2. FTIR Spectra of a) Ch and TMC b) PAA, TMC and TMC/PAA c) TMC/PAA and TMC/PAA/Ag.

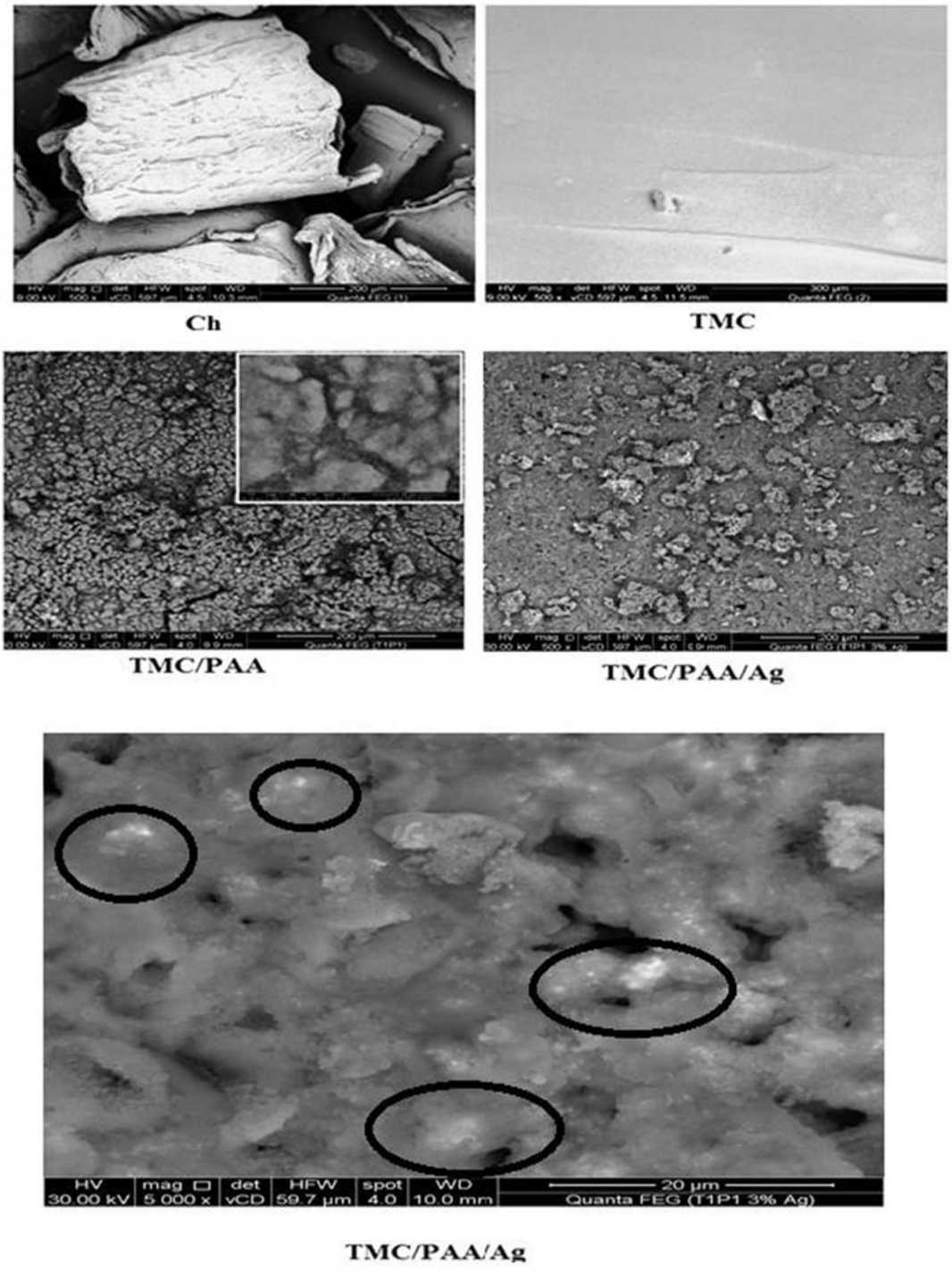

Fig. 3. SEM images of Ch, TMC, TMC/PAA and TMC/PAA/Ag.

(×5000) due to the presence of Ag nanoparticles throughout polymeric matrix.

4.4. Transmission electron microscopy (TEM)

Transmission electron microscopy images and their histograms of particles size distribution of Ag NPs with different weight ratios 1%, 2% and 3% were shown in Fig. 4(a–c). The results indicated that the synthesized Ag NPs were spherical in shape and polydispersed throughout the thin layer of polymeric matrix, while the histograms (Fig. 4d–f) showed two particle diameter regions, small Ag NPs particles of diameter range (5–30 nm) and large particles of diameter >30 nm. It was shown that small particle diameter range (5–30 nm) dominated nanocomposites with less Ag weight ratio (1% Ag NPs), while the diameter range of particles increased with increasing the Ag weight ratios, so nanocomposites with 2% Ag NPs had particles of diameter range (30–45 nm) and 3%Ag NPs nanocomposites had particles diameter of range (30–65 nm).

The elemental analysis of TMC/PAA/Ag (3%) was studied using EDX (energy dispersive X-ray analysis) and the results were illustrated in (Fig. 5). The EDX pattern showed the presence of Ag, this indicated the synthesis of Ag NPs.

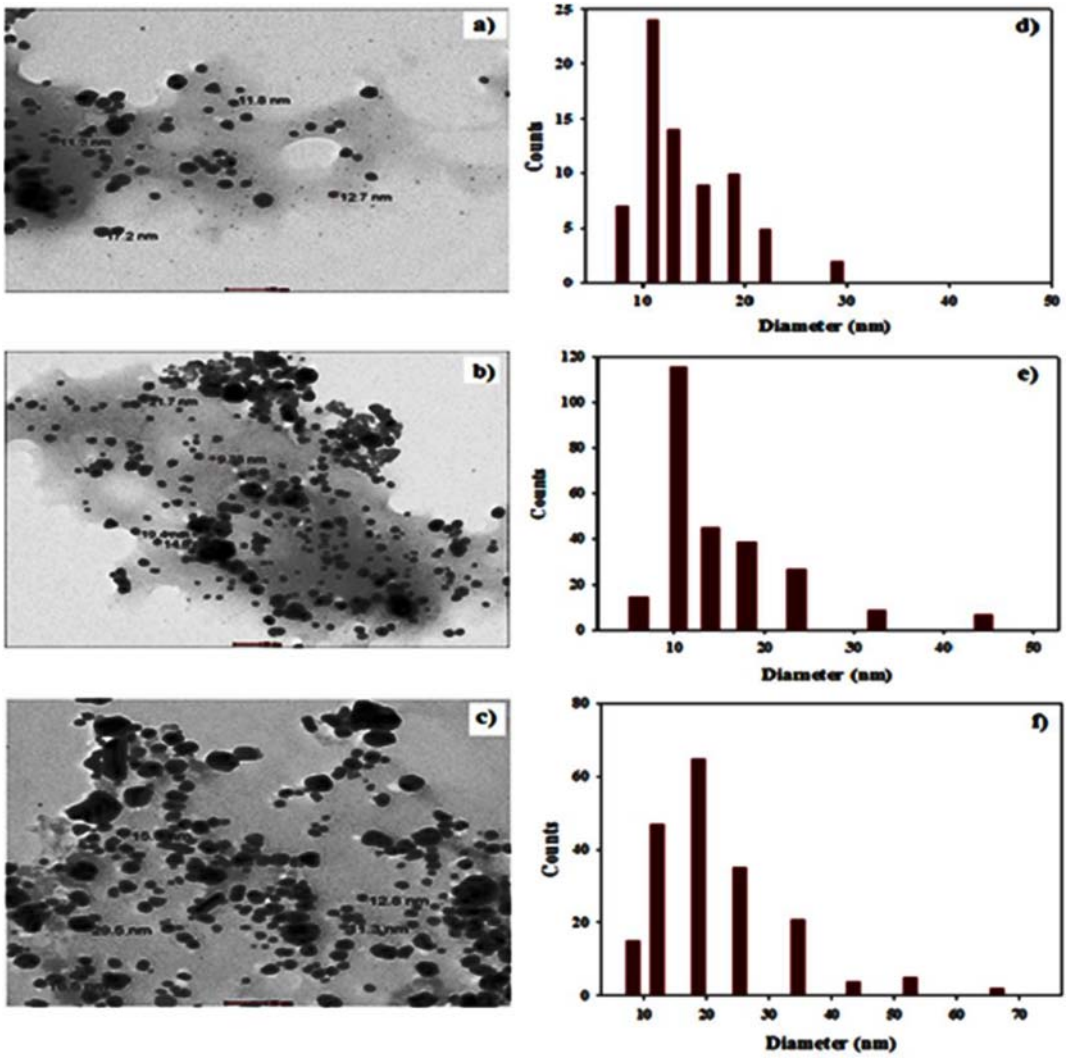

Fig. 4. TEM images of nanocomposites with a) 1% Ag b) 2% Ag c) 3% Ag with histograms of particle size distributions of d) 1% e) 2% f) 3% Ag nanoparticles.

4.5. X-ray diffraction (XRD)

X-ray diffraction (XRD) patterns of TMC, TMC/PAA (PEC) and TMC/PAA/Ag (3%) nanocomposites are illustrated in Fig. 6(a). XRD pattern of TMC showed one broad diffraction peak at 2θ = 19.5° with small intensity, so, TMC had less crystalline nature due to the presence of *N*-methyl groups on TMC chains that led to the destruction of the intermolecular hydrogen bonding among TMC chains. In addition, the XRD pattern of TMC/PAA (PEC) showed one broad diffraction peak at 2θ = 19° with more intensity than the same diffraction peak in TMC alone due to the presence of H-bonding and electrostatic interactions between TMC and PAA chains, so, TMC/PAA (PEC) was more crystalline than TMC, while the XRD pattern of TMC/PAA/Ag (3%) nanocomposite indicated the disappearance of the broad diffraction peak of TMC/PAA (PEC) - Fig. 6(a) - after preparing Ag nanoparticles which indicated the destruction of the crystalline region of TMC/PAA through the preparation of Ag (NPs) in situ. This observation was similar to the green synthesis of Ag nanoparticles in situ within bagasse and in presence of

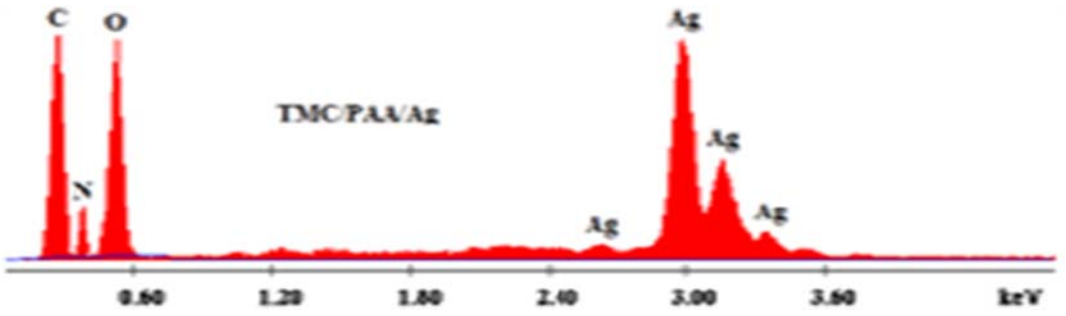

Fig. 5. EDX pattern for TMC/PAA/Ag.

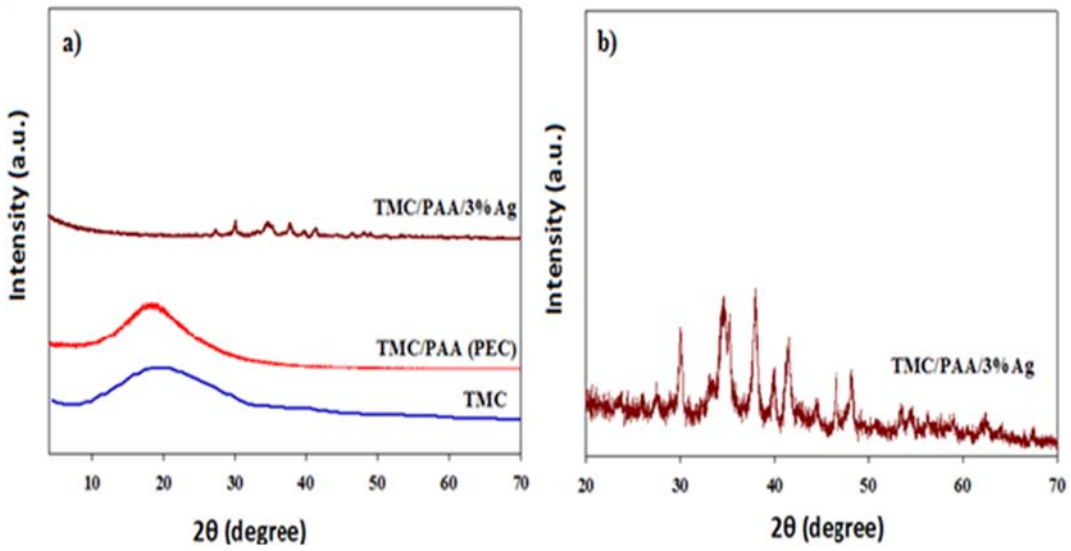

Fig. 6. XRD patterns of a) TMC, TMC/PAA (PEC) and TMC/PAA/Ag nanocomposites and b) TMC/PAA/Ag nanocomposites (magnification).

quaternized chitosan/rectorite [10, 20]. Fig. 6(b) showed different diffraction peaks at 2θ = 29.9°, 34.5°, 39.7°, 41.5°, 46.5° and 49.2° that indicated the crystalline nature of Ag nanoparticles that were prepared by green synthesized method.

4.6. Antimicrobial activity

Results of antimicrobial activity of TMC, PAA, TMC/PAA (PEC) and TMC/PAA/Ag nanocomposites against tested pathogenic

Table 1A
Antimicrobial activity of TMC, PAA, TMC/PAA (PEC) and TMC/PAA/Ag nanocomposites with different weight ratios (1%, 2% and 3%) against pathogenic microorganisms.

Samples	Inhibition zone diameter (mm)					
	Gram-negative bacteria		*Gram-positive* bacteria		Fungi	
	E. coli	*K. pneumoniae*	*S. aureus*	*B. subtilis*	*A. fumigatus*	*G. candidum*
Gentamicin (Reference)	22.3 ± 0.18	25.8 ± 0.58	–	–	–	–
Ampicillin (Reference)	–	–	27.4 ± 0.18	32.4 ± 0.10	–	–
Amphotericin B (Reference)	–	–	–	–	23.7 ± 0.10	28.7 ± 0.20
TMC	9.3 ± 1.50	12.3 ± 1.20	11.6 ± 0.63	13.7 ± 0.58	11.5 ± 1.20	10.2 ± 0.72
PAA	13.6 ± 0.63	15.2 ± 0.58	14.9 ± 1.20	16.3 ± 1.50	14.2 ± 1.50	13.6 ± 0.63
TMC/PAA (PEC)	19.5 ± 1.50	21.2 ± 0.58	20.4 ± 1.20	22.3 ± 0.58	18.2 ± 0.58	21.9 ± 0.63
TMC/PAA/ 1% Ag	21.6 ± 0.72	22.4 ± 1.20	21.6 ± 0.37	23.4 ± 0.58	19.6 ± 1.20	22.5 ± 1.50
TMC/PAA/ 2% Ag	23.2 ± 0.63	23.9 ± 1.50	22.5 ± 0.72	25.4 ± 1.50	21.2 ± 0.63	23.4 ± 0.58
TMC/PAA/ 3% Ag	23.7 ± 1.50	25.2 ± 1.20	24.3 ± 0.63	26.3 ± 0.72	23.3 ± 1.20	25.5 ± 0.58

Table 1B
MIC (μg mL^{-1}) of TMC, PAA, TMC/PAA (PEC) and TMC/PAA/Ag nanocomposites with different weight ratios (1%, 2% and 3%) against pathogenic microorganisms.

Samples	MIC (μg mL^{-1})					
	Gram-negative bacteria		*Gram-positive* bacteria		Fungi	
	E. coli	*K. pneumoniae*	*S. aureus*	*B. subtilis*	*A. fumigatus*	*G. candidum*
Gentamicin (Reference)	0.98	0.49	–	–	–	–
Ampicillin (Reference)	–	–	0.49	0.49	–	–
Amphotericin B (Reference)	–	–	–	–	0.98	0.49
TMC	250	250	250	125	250	250
PAA	125	62.50	62.50	62.50	125	125
TMC/PAA PEC	3.90	1.95	3.90	0.98	7.81	1.95
TMC/PAA/ 1% Ag	1.95	0.98	1.95	0.98	3.90	0.98
TMC/PAA/ 2% Ag	0.98	0.98	0.98	0.49	1.95	0.98
TMC/PAA/ 3% Ag	0.98	0.49	0.98	0.49	0.98	0.49

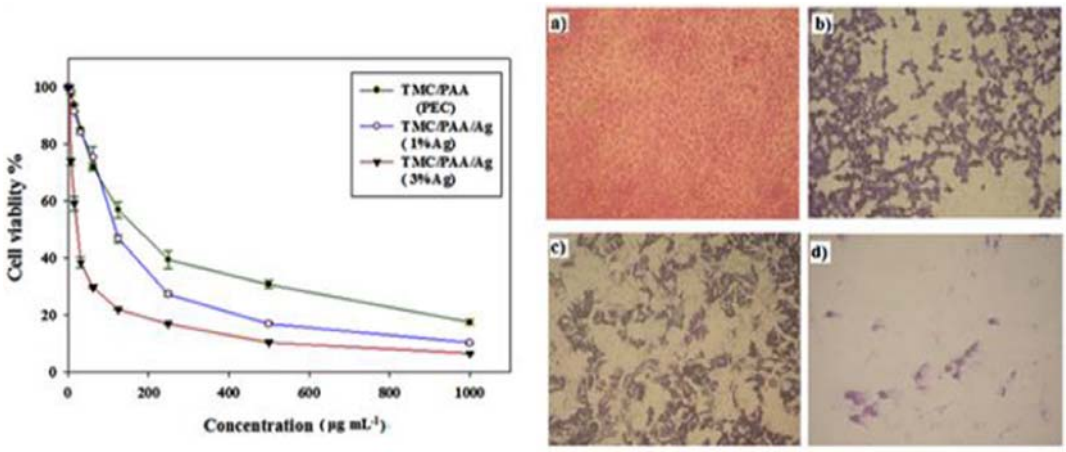

Fig. 7. Cytotoxicity effects of TMC/PAA (PEC) and TMC/PAA/Ag nanocomposites on HCT - 116 cells after incubation 24 h (right) a) Control sample (untreated cells) b) cells treated by TMC/PAA (PEC) c) cells treated by TMC/PAA/Ag (1%) d) cells treated by TMC/PAA/Ag (3%) nanocomposites at concentration 1000 μg mL^{-1}.

microorganisms using Agar well diffusion method in presence of reference drugs are tabulated in Tables 1A and 1B. The most acceptable mechanism of chitosan and *N*-quaternized chitosan derivatives is the electrostatic attraction forces between the positive charges of *N*-quaternized ($-N^+R_3$) groups along chitosan chains and the negative charges on microbial cell membrane [29, 58, 59]. So, TMC has antimicrobial activity against both pathogenic bacteria and fungi due to the electrostatic forces between *N*-quaternized ($-N^+(CH_3)_3$) groups on TMC chains (degree of quaternization DQ 70%) and the electronegative charges on the cytoplasmic membrane microorganisms cell surface. The cytoplasmic cell membrane contains proteins and phospholipids and polymer chains may cause strong interactions with cell membrane through H- bonding interactions [59, 60]. The interaction of TMC was similar to the interaction between quaternized carboxymethyl chitosan with negative charges on Algae cell surface that led to Algae inhibition [61]. Also, the results showed good antimicrobial activity for PAA due to H-bonding interactions of carboxylic acid (-COOH) groups on PAA backbone with the cytoplasmic cell membrane of microorganisms. The results indicated that TMC/PAA (PEC) had higher antimicrobial activity than parent TMC and PAA, because PEC was prepared in acidic medium so it increased the cationic charges on $-N^+H_2CH_3$ and $-N^+H(CH_3)_2$ groups, in addition to $-N^+(CH_3)_3$ on TMC chains, which increases the electrostatic interactions with the negatively charged cell membranes of the microorganisms. After dipping AgNPs throughout TMC/PAA matrix, the antimicrobial activity against pathogenic bacteria and fungi increased with increasing AgNPs content % in polymeric matrix - Table 1(A). Ag NPs have good antimicrobial activity due to their interaction with both sulfur atoms found in cell membrane proteins and compounds containing phosphorus in cells, so they damage these cells through their attack on the respiratory chain with these cell division [10, 62]. Also, AgNPs have high antibacterial activity because of its high surface area that interacts with bacterial cell wall [63]. From suggested mechanisms, Ag NPs were proven to be better antimicrobial agents. Furthermore, the results of TMC/PAA with 3% Ag NPs showed the most antimicrobial activity with less MIC values-Table 1(B) in the range 0.49–0.98 μg·mL^{-1} that was similar to the investigated reference drugs.

4.7. Cell viability assays

Cytotoxicity effect of different concentrations (3.9, 7.8, 15.6, 31.25, 62.5, 125, 250, 500, 1000 μg mL^{-1}) of tested samples (TMC/PAA, TMC/PAA/Ag nanocomposites with Ag ratios (1% and 3% Ag) on cell viability of HCT-116 colon cancer cells was investigated and was represented by

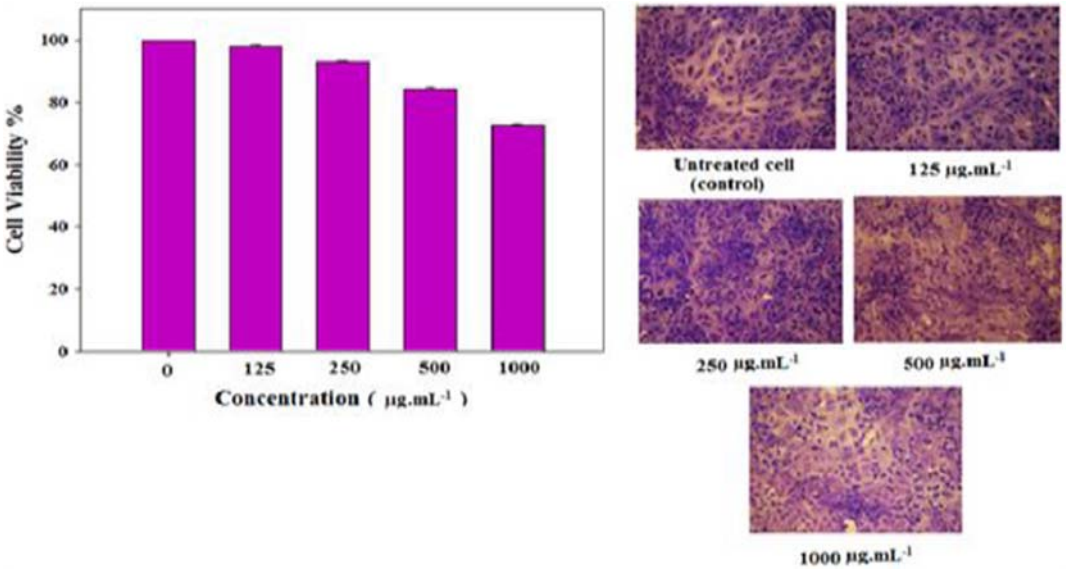

Fig. 8. Cytotoxicity effects of TMC/PAA/Ag (3%) nanocomposites on VERO cell lines at different concentrations compared to untreated cells and error bars represent the standard deviation (left), while images of VERO cell lines after incubation for 24 h with different nanocomposite concentrations (right).

dose response curve - (Fig. 7), which showed that the cytotoxicity effects of tested samples increased with increasing the concentration of samples, so at concentration 1000 μg mL^{-1}, there was a strong decrease in cell viability %. Fig. (7) showed that 500 μg mL^{-1} of TMC/PAA, TMC/PAA/Ag (1%) and TMC/PAA/Ag (3%) killed 69.2%, 83.1% and 89.6% of the cells, respectively. While, 1000 μg mL^{-1} of previous samples killed 82.6%, 89.8% and 93.5% of the cells after 24 h incubation. Moreover, IC_{50} was calculated for tested samples. IC_{50} of TMC/PAA was 174 μg mL^{-1}, TMC/PAA/Ag nanocomposites was 118 μg mL^{-1} (for 1% Ag) and 22.5 μg mL^{-1} (for 3% Ag). Cytotoxicity data confirmed that TMC/PAA/Ag (3%) had the highest cytotoxicity effect (the less cell viability %). The data showed that cytotoxicity assays of TMC/PAA and its Ag nanocomposites were better than others in literature (TMC-g-PVA) and (TMC/Alginate, ALG, and TMC/ALG/Ag nanocomposites) [11, 64]. The images of cancer cells that were treated with the tested samples are shown in Fig. (7), illustrating the various morphological changes that occurred to cancer cells after treatment with 1000 μg mL^{-1} concentrations of the samples due to their cytotoxic effects. Cell shrinkage occurred and the cells became smaller in size and the cytoplasm became condensed and more tightly packed. Cytotoxic effect increases with the increase in Ag content (%Ag). The cytotoxicity of TMC/PAA/Ag (3%) nanocomposite was also studied on African green monkey kidney cell lines (VERO cells) and the results are illustrated in Fig. (8). The results showed that TMC/PAA/Ag (3%) nanocomposite had less cytotoxicity effect on healthy VERO cell lines. IC_{50} of nanocomposite was much higher than 1000 μg mL^{-1}, so the results exhibited no significant destructive effect for the nanocomposite was observed on VERO cell lines. This observation was in agreement with literature [11].

5. Conclusion

Water soluble PEC based on *N,N,N*-trimethyl chitosan chloride (TMC) as a cationic polymer and poly(acrylic acid), PAA, as an anionic polymer was synthesized. The structure of PEC was proven with different analysis tools such as: ^{1}H-NMR, FTIR, XRD and SEM techniques. The results showed that PEC formed through electrostatic interactions between *N*-quaternized groups in TMC and carboxylate anion groups in PAA. Green synthesis of TMC/PAA/Ag nanocomposites with different weight ratios of Ag (1%, 2% and 3%) depends on hydroxyl groups on TMC as a self-reducing agent in presence of PAA as a self-stabilizing agent.

Synthesis of TMC/PAA/Ag nanocomposites was proven using FTIR, SEM, TEM/EDX and XRD techniques. The results confirmed the preparation of AgNPs through PEC chains. While, TEM and its histograms showed that the synthesized Ag NPs were spherical in shape and polydispersed having different particle diameter ranges, a small size range (5–30 nm) that dominated in TMC/PAA/Ag nanocomposites with 1% Ag and two large size diameter ranges, (30–45 nm) for 2% Ag and (30–65 nm) for 3% Ag nanocomposites.

Antimicrobial activity results showed that TMC/PAA (PEC) had higher antimicrobial activity against pathogenic *Gram-positive* and *Gram-negative* bacteria and fungi than TMC and PAA alone.

However, TMC/PAA/Ag nanocomposites had the highest antimicrobial activity compared with the tested reference drugs and its antimicrobial activity increased with increasing Ag weight ratio (%).

Cytotoxicity assays data of TMC/PAA and its Ag nanocomposites were better than others used before in literature. It was also shown that TMC/PAA/Ag (3%) had the highest cytotoxicity effect (the less cell viability %) on Colon cancer line. Also, the results exhibited no significant destructive effect of the nanocomposites on VERO cell lines.

References

[1] M.E. Chase-Topping, T. Rosser, L.J. Allison, E. Courcier, J. Evans, I.J. McKendrick, et al., Pathogenic potential to humans of bovine *Escherichia coli* O26, Scotland, Emerg. Infect. Dis. 18 (2012) 439–448.

[2] P. Cartwright, U. Somerset, Bacillus subtilis–identification and safety, Microbiology 105 (2009) 510–520.

[3] K.E. Holt, H. Wertheim, R.N. Zadoks, S. Baker, C.A. Whitehouse, D. Dance, et al., Genomic analysis of diversity, population structure, virulence, and antimicrobial resistance in *Klebsiella pneumoniae*, an urgent threat to public health, Proc. Natl. Acad. Sci. 112 (2015) (E3574-E81).

[4] H. Jolink, R. de Boer, P. Hombrink, R.E. Jonkers, J.T. van Dissel, J.F. Falkenburg, et al., Pulmonary immune responses against *Aspergillus fumigatus* are characterized by high frequencies of IL-17 producing T-cells, J. Inf. Secur. 74 (2017) 81–88.

[5] Y. Chang, H. Yoon, D.-H. Kang, P.-S. Chang, S. Ryu, Endolysin LysSA97 is synergisticwith carvacrol in controlling Staphylococcus aureus in foods, Int. J. Food Microbiol. 244 (2016) 19–26.

[6] S. Saha, A. Pal, S. Kundu, S. Basu, T. Pal, Photochemical green synthesis of calcium-alginate-stabilized Ag and Au nanoparticles and their catalytic application to 4-nitrophenol reduction, Langmuir 26 (2009) 2885–2893.

[7] S.B. Kalidindi, B.R. Jagirdar, Nanocatalysis and prospects of green chemistry, ChemSusChem 5 (2012) 65–75.

[8] M. Zayats, A.B. Kharitonov, S.P. Pogorelova, O. Lioubashevski, E. Katz, I. Willner, Probing photoelectrochemical processes in Au— CdS nanoparticle arrays by surface Plasmon resonance: application for the detection of acetylcholine esterase inhibitors, J. Am. Chem. Soc. 125 (2003) 16006–16014.

[9] A.F. Martins, J.P. Monteiro, E.G. Bonafé, A.P. Gerola, C.T. Silva, E.M. Girotto, et al., Bactericidal activity of hydrogel beads based on N, N, N-trimethyl chitosan/alginate complexes loaded with silver nanoparticles, Chin. Chem. Lett. 26 (2015) 1129–1132.

[10] J. Luo, M. Xie, X. Wang, Green fabrication of quaternized chitosan/rectorite/Ag NP nanocomposites with antimicrobial activity, Biomed. Mater. 9 (2014), 011001.

[11] A.F. Martins, H.D. Follmann, J.P. Monteiro, E.G. Bonafé, S. Nocchi, C.T. Silva, et al., Polyelectrolyte complex containing silver nanoparticles with antitumor property on Caco-2 colon cancer cells, Int. J. Biol. Macromol. 79 (2015) 748–755.

[12] M. Asif, M.A. Al-Mansoub, M.S.S. Khan, A.H.S. Yehya, M.O. Ezzat, C.E. Oon, et al., Molecular mechanisms responsible for programmed cell death-inducing attributes of terpenes from Mesua ferrea stem bark towards human colorectal carcinoma HCT 116 cells, J. Appl. Biomed. 15 (2017) 71–80.

[13] M.P. Singh, J. Han, S.C. Kang, 3′, 5-dihydroxy-3, 4′, 7-trimethoxyflavone-induces ER-stress-associated HCT-116 programmed cell death via redox signaling, Biomed Pharmacother 88 (2017) 151–161.

[14] M.M. Center, A. Jemal, E. Ward, International trends in colorectal cancer incidence rates, Cancer Epidemiol. Prev. Biomark. 18 (2009) 1688–1694.

[15] A.S. Soliman, M.L. Bondy, B. Levin, S. El-Badawy, H. Khaled, A. Hablas, et al., Familial aggregation of colorectal cancer in Egypt, Int. J. Cancer 77 (6) (1998) 811.

[16] V. Boncheva, S. Bonney, S.E. Brooks, M. Tangney, G. O'sullivan, A. Mirnezami, et al., New targets for the immunotherapy of colon cancer—does reactive disease hold the answer? Cancer Gene Ther. 20 (2013) 157–168.

[17] A. Jemal, F. Bray, M.M. Center, J. Ferlay, E. Ward, D. Forman, Global cancer statistics, CA Cancer J. Clin. 61 (2011) 69–90.

[18] H. Zhang, M. Wu, A. Sen, Silver nanoparticle antimicrobials and related materials, Nano-Antimicrobials, Springer 2012, pp. 3–45.

[19] S. Das, D. Sasmal, S. Pal, H. Kolya, A. Pandey, T. Tripathy, Starch based biodegradable graft copolymer for the preparation of silver nanoparticles, Int. J. Biol. Macromol. 81 (2015) 83–90.

[20] Z. Shen, G. Han, X. Wang, J. Luo, R. Sun, An ultra-light antibacterial bagasse–AgNP aerogel, J. Mater. Chem. B 5 (2017) 1155–1158.

[21] S.C. Boca, M. Potara, A.-M. Gabudean, A. Juhem, P.L. Baldeck, S. Astilean, Chitosan-coated triangular silver nanoparticles as a novel class of biocompatible, highly effective photothermal transducers for in vitro cancer cell therapy, Cancer Lett. 311 (2011) 131–140.

[22] V.K. Sharma, R.A. Yngard, Y. Lin, Silver nanoparticles: green synthesis and their antimicrobial activities, Adv. Colloid Interf. Sci. 145 (2009) 83–96.

[23] W. Xu, W. Jin, L. Lin, C. Zhang, Z. Li, Y. Li, et al., Green synthesis of xanthan conformation-based silver nanoparticles: antibacterial and catalytic application, Carbohydr. Polym. 101 (2014) 961–967.

[24] S. Asghari, S.A. Johari, J.H. Lee, Y.S. Kim, Y.B. Jeon, H.J. Choi, et al., Toxicity of various silver nanoparticles compared to silver ions in *Daphnia magna*, J. Nanobiotechnol. 10 (2012) 14.

[25] H. Bar, D.K. Bhui, G.P. Sahoo, P. Sarkar, S.P. De, A. Misra, Green synthesis of silver nanoparticles using latex of *Jatropha curcas*, Colloids Surf. A Physicochem. Eng. Asp. 339 (2009) 134–139.

[26] A. Mishra, N.K. Kaushik, M. Sardar, D. Sahal, Evaluation of antiplasmodial activity of green synthesized silver nanoparticles, Colloids Surf. B: Biointerfaces 111 (2013) 713–718.

[27] S. Li, Y. Shen, A. Xie, X. Yu, L. Qiu, L. Zhang, et al., Green synthesis of silver nanoparticles using *Capsicum annuum* L. extract, Green Chem. 9 (8) (2007) 852.

[28] A.F. Martins, S.P. Facchi, H.D. Follmann, A.G. Pereira, A.F. Rubira, E.C. Muniz, Antimicrobial activity of chitosan derivatives containing N-quaternized moieties in its backbone: a review, Int. J. Mol. Sci. 15 (2014) 20800–20832.

[29] R.R. Mohamed, M.H. Abu Elella, M.W. Sabaa, Synthesis, characterization and applications of N-quaternized chitosan/poly (vinyl alcohol) hydrogels, Int. J. Biol. Macromol. 80 (2015) 149–161.

[30] A.F. Martins, S.P. Facchi, H.D. Follmann, A.P. Gerola, A.F. Rubira, E.C. Muniz, Shielding effect of 'surface ion pairs' on physicochemical and bactericidal properties of N, N, N-trimethyl chitosan salts, Carbohydr. Res. 402 (2015) 252–260.

[31] Z. Ni, Z. Wang, L. Sun, B. Li, Y. Zhao, Synthesis of poly acrylic acid modified silver nanoparticles and their antimicrobial activities, Mater. Sci. Eng. C 41 (2014) 249–254.

[32] R.R. Mohamed, M.H. Abu Elella, M.W. Sabaa, Cytotoxicity and metal ions removal using antibacterial biodegradable hydrogels based on N-quaternized chitosan/poly (acrylic acid), Int. J. Biol. Macromol. 98 (2017) 302–313.

[33] A. Henglein, Colloidal silver nanoparticles: photochemical preparation and interaction with O2, CCl4, and some metal ions, Chem. Mater. 10 (1998) 444–450.
[34] D. de Britto, O.B. Assis, A novel method for obtaining a quaternary salt of chitosan, Carbohydr. Polym. 69 (2007) 305–310.
[35] U. Mithun, B. Vishalakshi, J. Karthika, Preparation and characterization of polyelectrolyte complex of N, N, N-trimethyl chitosan/gellan gum: evaluation for controlled release of ketoprofen, Iran. Polym. J. 25 (2016) 339–348.
[36] J. Verma, J. Kanoujia, P. Parashar, C.B. Tripathi, S.A. Saraf, Wound healing applications of sericin/chitosan-capped silver nanoparticles incorporated hydrogel, Drug Deliv. Transl. Res. 7 (2017) 77–88.
[37] R. Miles, S. Amyes, Laboratory control of antimicrobial therapy. Mackie and McCartney practical medical, Microbiology 14 (1996) 151–178.
[38] K.R. K Saini, S.A. Choudhary, Y.C. Joshi, P. Joshi, Solvent free synthesis of chalcones and their antibacterial activities, J. Chemother. 2 (2005) 224–227.
[39] M. Bhuiyan, M. Hossain, M. Mahmud, M. Al-Amin, Microwave-assisted efficient synthesis of chalcones as probes for antimicrobial activities, Chem. J. 1 (2011) 21–28.
[40] T. Mosmann, Rapid colorimetric assay for cellular growth and survival: application to proliferation and cytotoxicity assays, J. Immunol. Methods 65 (1983) 55–63.
[41] V. Gangadevi, J. Muthumary, Preliminary studies on cytotoxic effect of fungal taxol on cancer cell lines, Afr. J. Biotechnol. 6 (2007).
[42] H.E. Salama, G.R. Saad, M.W. Sabaa, Synthesis, characterization, and biological activity of cross-linked chitosan biguanidine loaded with silver nanoparticles, J. Biomater. Sci. Polym. Ed. 1 (2016).
[43] F. Tian, Y. Liu, K. Hu, B. Zhao, Study of the depolymerization behavior of chitosan by hydrogen peroxide, Carbohydr. Polym. 57 (2004) 31–37.
[44] Ö.V. Rúnarsson, C. Malainer, J. Holappa, S.T. Sigurdsson, M. Másson, Tert-Butyldimethylsilyl O-protected chitosan and chitooligosaccharides: useful precursors for N-modifications in common organic solvents, Carbohydr. Res. 343 (2008) 2576–2582.
[45] W. Sajomsang, P. Gonil, S. Saesoo, Synthesis and antibacterial activity of methylated N-(4-N, N-dimethylaminocinnamyl) chitosan chloride, Eur. Polym. J. 45 (2009) 2319–2328.
[46] M. Avadi, A. Sadeghi, A. Tahzibi, K. Bayati, M. Pouladzadeh, M. Zohuriaan-Mehr, et al., Diethylmethyl chitosan as an antimicrobial agent: synthesis, characterization and antibacterial effects, Eur. Polym. J. 40 (2004) 1355–1361.
[47] T. Xu, M. Xin, M. Li, H. Huang, S. Zhou, J. Liu, Synthesis, characterization, and antibacterial activity of N, O-quaternary ammonium chitosan, Carbohydr. Res. 346 (2011) 2445–2450.
[48] A. Liu, I. Honma, M. Ichihara, H. Zhou, Poly (acrylic acid)-wrapped multi-walled carbon nanotubes composite solubilization in water: definitive spectroscopic properties, Nanotechnology 17 (2006) 2845.
[49] J. Dai, H. Yan, H. Yang, R. Cheng, Simple method for preparation of chitosan/poly (acrylic acid) blending hydrogel beads and adsorption of copper (II) from aqueous solutions, Chem. Eng. J. 165 (2010) 240–249.
[50] E. de Souza Costa-Júnior, M.M. Pereira, H.S. Mansur, Properties and biocompatibility of chitosan films modified by blending with PVA and chemically crosslinked, J. Mater. Sci. Mater. Med. 20 (2009) 553–561.
[51] H.S. Mansur, C.M. Sadahira, A.N. Souza, A.A. Mansur, FTIR spectroscopy characterization of poly (vinyl alcohol) hydrogel with different hydrolysis degree and chemically crosslinked with glutaraldehyde, Mater. Sci. Eng. C 28 (2008) 539–548.
[52] D. de Britto, O.B. de Assis, Synthesis and mechanical properties of quaternary salts of chitosan-based films for food application, Int. J. Biol. Macromol. 41 (2007) 198–203.
[53] K. Sharma, B. Kaith, V. Kumar, S. Kalia, V. Kumar, H. Swart, Water retention and dye adsorption behavior of Gg-cl-poly (acrylic acid-aniline) based conductive hydrogels, Geoderma 232 (2014) 45–55.
[54] Y. Zheng, D. Huang, A. Wang, Chitosan-g-poly (acrylic acid) hydrogel with crosslinked polymeric networks for Ni 2+ recovery, Anal. Chim. Acta 687 (2011) 193–200.
[55] Z. Hooshyar, G.R. Bardajee, A novel dual thermo-and pH-responsive silver nanocomposite hydrogel as a drug delivery system, J. Iran. Chem. Soc. 14 (2017) 541–549.
[56] I. El-Sherbiny, E. Salih, F. Reicha, New trimethyl chitosan-based composite nanoparticles as promising antibacterial agents, Drug Dev. Ind. Pharm. 42 (2016) 720–729.
[57] H.E. Salama, G.R. Saad, M.W. Sabaa, Synthesis, characterization, and biological activity of cross-linked chitosan biguanidine loaded with silver nanoparticles, J. Biomater. Sci. Polym. Ed. 27 (2016) 1880–1898.
[58] T. Ikeda, H. Hirayama, H. Yamaguchi, S. Tazuke, M. Watanabe, Polycationic biocides with pendant active groups: molecular weight dependence of antibacterial activity, Antimicrob. Agents Chemother. 30 (1986) 132–136.
[59] M. Kong, X.G. Chen, K. Xing, H.J. Park, Antimicrobial properties of chitosan and mode of action: a state of the art review, Int. J. Food Microbiol. 144 (2010) 51–63.
[60] C.H. Kim, J.W. Choi, H.J. Chun, K.S. Choi, Synthesis of chitosan derivatives with quaternary ammonium salt and their antibacterial activity, Polym. Bull. 38 (1997) 387–393.
[61] J. Cai, W. Ye, X. Wang, W. Lin, Q. Lin, Q. Zhang, et al., Preparation of copper-chelate quaternized carboxymethyl chitosan/organic rectorite nanocomposites for algae inhibition, Carbohydr. Polym. 151 (2016) 130–134.
[62] M. Rai, A. Yadav, A. Gade, Silver nanoparticles as a new generation of antimicrobials, Biotechnol. Adv. 27 (2009) 76–83.
[63] J.-Y. Maillard, P. Hartemann, Silver as an antimicrobial: facts and gaps in knowledge, Crit. Rev. Microbiol. 39 (2013) 373–383.
[64] A.F. Martins, P.V. Bueno, H.D. Follmann, S.R. Nocchi, C.V. Nakamura, A.F. Rubira, et al., Synthesis, characterization, and cytotoxicity of TMC-graft-poly (vinyl alcohol) copolymers, Carbohydr. Res. 381 (2013) 153–160.